Influence of reflecting boundaries and finite interfacial thickness on the coherent backscattering cone

Mark Ospeck and Seth Fraden
Martin Fisher School of Physics, Brandeis University, Waltham, Massachusetts 02254
(Received 30 April 1993; revised manuscript received 13 December 1993)

We investigate the effect of reflecting boundary conditions on the shape of the coherent backscattering (CB) cone of light by measuring the CB cone from a suspension of microspheres as a function of the thickness of the glass window containing the sample. The reflection from the air-glass interface is observed to narrow the cone, as previously predicted and observed; however, the finite thickness of the window introduces a slope discontinuity in the CB cone. The dominant contribution to the cone for angles less than the kink is from reflected light, while the cone at angles higher than the kink arises from light that directly leaves the sample. Thus the study of the CB cone as a function of window thickness offers an experimental method of separating the component of the cone due to interfacial reflectivity from the directly backscattered component. Monte Carlo simulations of the path length distribution of multiply scattered light were performed and compared well with both measurement and theories incorporating reflecting interfaces. It was found that under certain circumstances an interface of finite width lowered the CB cone height. Additionally, high quality measurements of the CB cone from Mie scatterers revealed an anisotropy in the cone similar to the case of Rayleigh spheres. Finally, the influence of reflecting boundaries on the decay of the temporal autocorrelation function and the height of the CB cone were investigated.

PACS number(s): 42.25.Kb, 42.25.Gy

I. INTRODUCTION

Weak localization of light concerns an optical memory effect of a random medium, in which the photon's inbound $\bar{k}$ vector is "remembered" by the random sample [1,2]. The scattered wave intensity is then observed to be approximately doubled within a narrow cone about the $-\bar{k}$ direction. The photon diffusion approximation has proved successful in explaining this coherent backscattering (CB) cone in the weak scattering limit $ql \gg 1$, where q is the magnitude of the scattering transfer wave vector and l is the photon mean free path [3–5].

In real space, the diffusion approximation views the CB cone as being generated by pairs of point sources of the electric field, which are located on the interface of the medium where the photons enter and exit the interface. The diffusion approximation concerns itself with calculating the distribution of separations of these entrance and exit points (we denote the separation of these points as ρ) in order to obtain the shape of the CB cone. In analogy to a pair of Young's slits, the angular width of the cone is inversely proportional to the average value of ρ, and in the diffusion approximation $\langle\rho\rangle \sim l^*$, with l^* the transport mean free path of the photon.

Certain difficulties had occurred in the past with the diffusion approximation because boundary conditions had not been dealt with adequately. The early theories neglected reflected light at the interface arising from the dielectric mismatch between the air and the scattering medium. It was subsequently noted by several authors [6–8] that the result of this neglect was the significant overestimation of the angular size of the CB cone because reinjection of the photon back into the sample increases $\langle\rho\rangle$. These same authors presented theories and experiments, which took into account reflectivity at the interface. We note that the intensity transport theory of Tsang and Ishimaru [9] did correctly incorporate the boundary conditions.

Experiments investigating the effect of interfacial reflectivity on the CB cone were first performed by Saulnier and Watson [10], who measured decreases in the CB cone width due to the sample cell's water-glass interface being coated with a silver mirror having a thin titania overcoat. They found good agreement between their experiments and the theory of Ref. [6]. The CB cones obtained with partially mirrored interfaces are noisy. When we repeated their experiments we found that the origin of the noise was due in large part to interference patterns created by the thin films on the mirrors and we observed that the quality of the CB cone decreased with increasing reflectivity. Another approach was adopted by Outer *et al.* [11], who measured CB cones from a solid-sample–fluid interface as a function of the index of refraction of the fluid, but the calculations of l^* in the solid sample and the value of the effective index of refraction of the solid scattering medium are difficult to perform.

In this paper we report a different method of probing the effect of reflecting boundary conditions on the shape of the CB cone. We measure the line shape of the CB cone from a 10% volume fraction colloidal suspension of identical microspheres as a function of the thickness of the window of the glass container, which is a case where the index of refraction of the scattering medium and l^* can be accurately calculated. Most of the light reflected back into the sample comes from the air-glass interface and this reflection is observed to narrow the cone width,

as previously predicted [6–8] and observed [10]. However, the finite thickness of the window introduces a slope discontinuity, or "kink" in the CB cone. The angle from backscattering of the kink is inversely proportional to the thickness of the glass window, but the detailed shape of the CB cone depends on the distribution of separations of the entering and exiting photons, which is also a function of window thickness. The dominant contribution to the cone for angles less than the kink is from reflected light, while the cone at angles higher than the kink arises from light that directly leaves the sample. Thus the study of the CB cone as a function of window thickness offers an experimental method of separating the component of the cone due to interfacial reflectivity from the directly backscattered component.

We have also performed several auxiliary experiments complementary to the ones discussed above. We measured the cone using apertured samples to eliminate all interfacial reflections and found that the measured Mie sphere cones compare well with the diffusion approximation calculation of Akkermans *et al.* [12], with the greatest exception being that the cone height is 1.82, in contrast to the theoretical prediction of 2.0. Additionally, high quality two-dimensional measurements of the CB cone from Mie scatterers revealed an anisotropy in the cone similar to the case of Rayleigh spheres. Finally, the influence of reflecting boundaries on the height of the CB cone and on the decay of the temporal autocorrelation function of scattered light were investigated.

We performed Monte Carlo simulations that calculated the path length distribution of multiply scattered light as a function of window thickness. The results compared well with both measurement and theories incorporating reflecting interfaces. These simulations go beyond the diffusion approximation because the exact boundary conditions are imposed (no trapping plane), but they still treat photons as scalar and ballistic particles rather than correctly as vector waves. We found that under certain circumstances, the finite width of the glass interface lowered the CB cone height. This may be important in understanding the unanswered question as to why observed CB cone heights are always less than two. In our simulations we also treat the case discussed theoretically [6–8] of the CB cone from a sample with an interface of zero thickness as a function of reflectivity and find good comparison with the theory of Freund and Berkovits [8]. In the limit of zero reflectivity we find that the line shape of the simulated CB cone is in good agreement with the diffusion approximation theory of Akkermans *et al.* [12] for the central portion of the cone, while there are small deviations in the high angle wings of the cone where the diffusion approximation breaks down.

The rest of the paper is as follows. Section II A will discuss our experimental setup and describe the anisotropy in the CB cone intensity for the case of Mie scattering spheres. Section II B contains the mechanism for how window thickness effects cone height and line shape. Section II C compares our simulation to both experiment and theory. Section II D contrasts reflection versus no-reflection cones and shows how the presence of a graded high index to low index interface could account for missing cone height. Our simulation is also compared against theories of cone width versus interface reflectivity. Section II E concerns itself with a second smaller cone height loss mechanism, and Sec. II F details a diffusing-wave spectroscopy experiment concerning itself with the variation in the decay rate of the intensity fluctuations as a function of the amount of reflected light.

II. EXPERIMENT

A. Vector nature of the multiple scattering

Figure 1 is a depiction of our experimental backscattering setup. An argon ion laser's green 514 nm line was vertically polarized (V) and then sent through a 5 μm spatial-filter–beam-expander combination. The resulting 20 mm diam Gaussian beam was next apertured down to 8 mm so as to have a uniform intensity and then reflected off a 50-50 beam splitter (3 mm thick, antireflection coated rear surface with $< 0.5\%$ reflectivity in order to eliminate the ghost beam) and then into a 12 mm aperture optical quality BK1 glass sample cell with 4 mm thick windows. The cell is apertured in such a way as to eliminate any reflected light from the glass-air interface from reaching the sample. The backscattered V-V light was collected by traversing back through the splitter and a vertical polarizer by a diffraction limited f/6.25, focal length 250 mm achromat focusing intensity onto a charge-coupled-device (CCD) camera. The CCD [13] had its sensor's glass faceplate removed in order to minimize interference patterns. A digitizer board [14] then sent the resulting cone pictures to a personal computer. Further image processing was done using IP labs commercial software [15].

Theory predicts a CB cone height of 1.88 for Rayleigh scatterers [4] having vertical polarization for both incom-

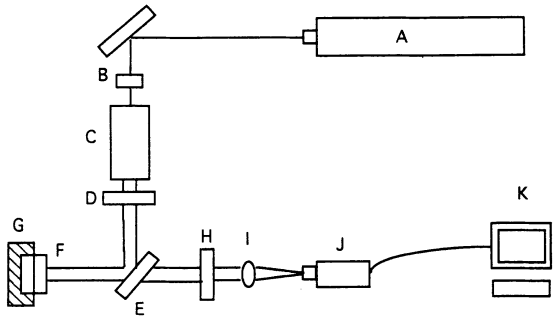

FIG. 1. Our experimental backscattering setup. *A* is the 514 nm argon-ion laser with vertically polarizing output head; *B* is the vertically polarizing crystal polarizer; *C* is the beam expander with a 5 μm spatial filter; *D* is the 8 mm diaphragm; *E* is the 50-50 beam splitter; *F* is the sample cell window, tilted slightly off axis to avoid specular reflection; *G* is the sample cell; *H* is the Polaroid vertically polarizing; *I* is the f/6.25, 250 mm focal length achromat; *J* is the CCD camera; and *K* is the digitizer board and Macintosh personal computer.

ing and outgoing light (V-V backscattering). This arises from the large fraction of single backscattering compared to total backscattering for Rayleigh particles. By the same reasoning one would expect a significantly higher Mie-scatterer cone, close in height to 2.0, because of the small fraction of single backscattered light from Mie scatterers. However, V-V backscattering experiments have been unable to produce a Mie cone much higher than 1.8 [4,16,17]. In several cases Mie cones with only a height of 1.6 are observed [2,4]. Wolf *et al.* [16] and van Albada *et al.* [4] discuss this Mie sphere CB cone height discrepancy, concluding that angle-independent scattering terms, such as single backscattering or closed loops, were the most likely suspects preventing the experimental Mie sphere cone from reaching a height above 1.85.

Figure 2(a) is a contour intensity plot of a Mie sphere CB cone from a 10% volume fraction 0.489 μm diam polystyrene colloidal sample reaching a coherent height of 0.82. This cone when referenced to a diffuse background at 10 mrad shows a coherent height of 0.78; however, at 10 mrad the cone wings are still descending towards the "true" diffuse background. Extrapolating these wings then yields the 0.82 coherent height. In this plate and the following plate the polarization direction is vertical or north-south (NS). The transport mean free path l^* is defined as the length over which the photon loses its direction memory. Mie calculations show the sample to have a mean free path $l = 3.9$ μm and a $l^* = 22$ μm. Note both l and l^* have been corrected for hard sphere correlations using the Percus-Yevick theory [16,18–20] to calculate the structure factor. The scattered intensity from a correlated suspension is modified from a suspension of uncorrelated particles by replacing the scattering form factor of a single sphere with a local hard sphere structure factor times the individual sphere's form factor. The mean free path l is increased by 32% due to the local structure factor of the hard sphere medium, but the transport mean free path is increased by only 6% due to the interparticle correlations. Increasing the local organization of the spheres lengthens both l and l^*.

The cone in Fig. 2(a) must be corrected for our detector response function which exhibits a small northwest-southeast (NW-SE) variation in gain, which increases to the southeast. Detector response was obtained by transmitting light through a multiply scattering colloidal suspension; the resulting Lambertian diffuser provided a flat intensity distribution for small forward scattering angles. The instrument corrected cone was then obtained by dividing the raw data [(Fig. 2(a)] by a normalized-to-unity detector response. The detector response NW-SE tilt was of the order of 10%. Our eight bit charge-coupled-device–digitizer combination had a dynamic range from 0 to 255. The dark level was adjusted to be 0.5 on average on this scale. Diffuse backgrounds for cone plates were set in the 90–100 range. Each cone plate was an average of 256 distinct cone speckle patterns spaced 1 s apart.

We Fourier transform this corrected cone in order to filter out an extraneous interference pattern lying in the east-west (EW) direction [Fig. 2(a)]. The Fourier components of said interference pattern were replaced with the local average value prior to inverse transforming, which then netted Fig. 2(b)'s corrected and filtered cone. Al-

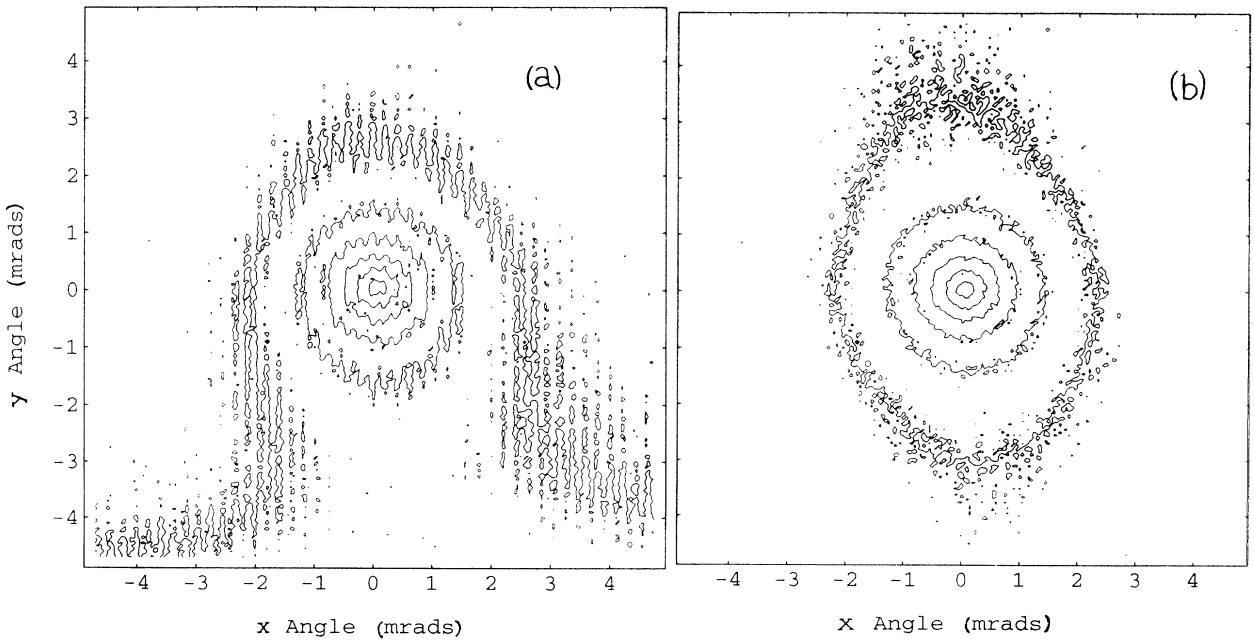

FIG. 2. (a) Ten milliradian square contour intensity plot of the raw data of a V-V backscatter cone from a 10% volume fraction polystyrene colloidal sample apertured to prevent reflected light from returning to the sample. Polarization direction is north-south. The dark level is approximately equal to 0.5. Each plate is an average of 256 cone speckle patterns spaced 1 s apart. (b) The detector-response-corrected, Fourier-filtered coherent backscatter cone. Polarization direction is north-south. For both (a) and (b) the contour spacing is equal to 14 , the lowest contour is equal to 97, and the highest contour is equal to 167.

ready in this picture a NS vs EW cone asymmetry is clearly visible. This asymmetry is displayed by plotting the intensities along the NS and EW directions in Fig. 3. The angular averaged cone is also plotted in Fig. 3 and a substantial reduction in noise is apparent. All other experimental CB cones shown below have also been similarly processed and angularly averaged. Since the anisotropy is only apparent in the tails of the cone, little error is introduced by this circular averaging of the scattered intensity.

First, an important definition: the perpendicular displacement $\overline{\rho}$ is defined as the vector between the first and last scatterer perpendicular to the incident wave vector $\overline{K}_{\rm in}$. The vector nature of the multiple scattering accounts for this increase in the angular width of the NS cone versus the EW cone. This effect, as explained by van Albada *et al.* [4,21], is a direct consequence of the electric dipole nature of the scatterings: the torus-shaped electric dipole scattering probability distribution insures that a polarization-preserving backscattering consisting of n scattering events will have a smaller perpendicular displacement parallel to its polarization than its perpendicular displacement perpendicular to this polarization. Example perpendicular displacements are the vectors $\overline{\rho_0\rho_1}$ and $\overline{\rho_0\rho_2}$ seen in Fig. 4. This anisotropy in perpendicular displacements will result in an elliptical cone, stretched in the direction of the polarization vector. van Albada *et al.* [4,21] both predicted and observed this vector memory effect for the low orders of Rayleigh backscattering. Contrary to expectations this effect is also found to hold for the large Mie spheres [4]. In Fig. 6 it is important to notice that the cone's inner contours are circular, while only the outer contour is elliptical: these inner contours correspond to small angles and long perpendicular displacements, while the outer contour corresponds to a short perpendicular displacement and a low order backscattering. This polarization anisotropy appears to be only a low order scattering effect [4,21].

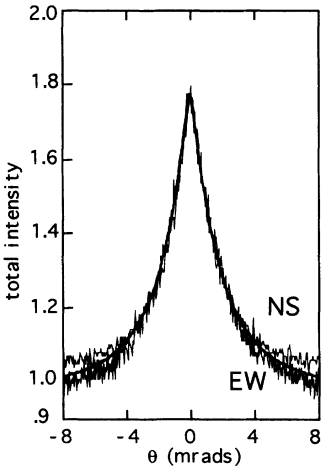

FIG. 3. Plot of the total intensity of the backscattering cone [Fig. 2(b)] where the background at 10 mrad was normalized to 1. The top curve is a NS slice through the cone from Fig. 2(b), while the bottom curve is an EW slice. Note the difference in wing levels for the two cuts due to the vector nature of the multiple scattering. The middle smoothed cone is a circular average of the entire $2D$ data set.

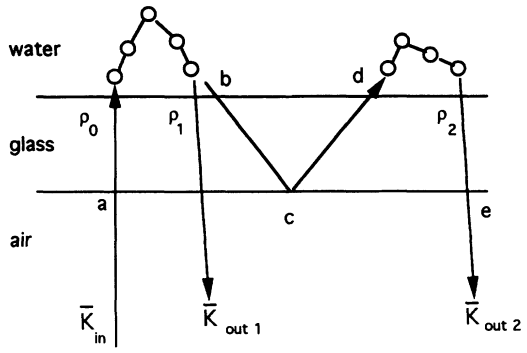

FIG. 4. Increase in multiple scattering perpendicular displacement from $\overline{\rho_0\rho_1}$ in loop 1 to $\overline{\rho_0\rho_2}$ in loop 2 due to a single glass-air reflection occurring approximately at the glass-air critical angle ($\theta_{\rm crit}$) of 42°. The photon experiences small reflection probabilities at points a, ρ_0, b, d, ρ_2, and e and a 100% reflection at point c. The net result for windows thick compared to l^* is a single-reflection peak in the path length distribution, having a perpendicular displacement $\overline{\rho_0\rho_2} \approx \overline{bd} = 2D\tan(\theta_{\rm crit})$, with D the window thickness.

B. Path length distribution versus window thickness

The coherent part of the CB cone $\alpha_c(q)$ can be expressed as an integral transform of its path length distribution $Q(\rho, L)$ [12,16]. $Q(\rho, L)$ is the probability of a scattering path having a total length L and a perpendicular displacement ρ. $Q(\rho)$, having been integrated with respect to L, is the probability of a scattering path having a perpendicular displacement ρ. $Q(\rho)$ is the relevant distribution for constructing the CB cone and $q_\perp \approx 2\pi\theta/\lambda$ is the projection of the transfer wave vector perpendicular to $K_{\rm in}$. The relation between $\alpha_c(q_\perp)$ and $Q(\rho)$ is [12,16]

$$\alpha_c(q_\perp) = \int\int Q(\rho)\exp(i\overline{q_\perp}\cdot\overline{\rho})d^2\rho \quad (1)$$

$$= \int 2\pi\rho Q(\rho)J_0(q_\perp\rho)d\rho. \quad (2)$$

In the diffusion approximation the function $Q(\rho, L)$ will have a Gaussian dependence on ρ [12]. Note that Fig. 2(b)'s asymmetric CB cone suggests a corresponding asymmetry in the NS versus EW perpendicular displacement distributions, i.e., $Q(\rho)_{\rm NS}$ and $Q(\rho)_{\rm EW}$.

Figure 4 shows schematically the relevant path length increase due to a single reflection from a sample's glass-air interface. A small multiple scattering perpendicular displacement $\overline{\rho_0\rho_1}$ will tend to be lengthened by $\overline{bd}$ to become $\overline{\rho_0\rho_2}$. Because a two-dimensional Fourier transform of this perpendicular displacement distribution $Q(\rho)$ gives the CB cone $\alpha_c(q)$, an additional peak in this $Q(\rho)$ distribution (here brought about by reflection from a thick window) will cause a slope discontinuity to appear in the cone. In our experiment we have changed the lo-

cation of such a peak in this perpendicular displacement distribution $Q(\rho)$ by varying the thickness of the sample cell's window.

We performed Monte Carlo multiple scattering computer simulations that calculated perpendicular displacement distributions $Q(\rho)$ and CB cones and then compared these cones against our experimental ones. The simulation modeled random-walking photons (not amplitudes) and took into account both the Mie form factor and the hard sphere Percus-Yevick [16,18–20] structure factor for 0.489 μm diam spheres at 10% volume fraction. Photons initially were incident normally to the interface and continued until scattering from a particle. The distance between each scattering event was an exponentially distributed random variable on the interval from one particle diameter to five times the mean free path l calculated to be 3.9 μm as described above. The scattering angle (ϕ, θ) was a uniformly distributed random variable on ϕ, the azimuthal angle, and a random variable distributed according to the form factor times the structure factor on θ, the in-scattering-plane angle between the incident and scattered wave vectors. In the simulation we assumed random polarization, so that the form factor was the average of the two polarization's Mie form factors [22]. This means that the photons are treated as scalar particles and thus no anisotropy in the cone will be observed. We neglected reflection, but not refraction at the colloid-glass interface and calculated reflection from the glass-air interface according to the angle-dependent Fresnel reflectivity equations. Again, we assumed that the light was completely depolarized at the interface and the Fresnel reflectivity coefficients were averaged over the two polarizations. This random polarization approximation is valid for the long scattering paths whose photons have met many different scattering planes while in the sample and have had their polarizations effectively scrambled by them. The short paths, however, would retain significant memory of their initial vertical polarization, as demonstrated by the elliptical outer contour of Fig. 2(b). The reflectivity of the water-glass interface is small because it is from an optically light to an optically dense media and therefore has no critical angle, resulting in a small average interface reflectivity ($< 10\%$). Typically each simulation would partition between 20 and 40 thousand photons according to their perpendicular displacement lengths, ρ independent of the final angle of exit of the photon from the sample. In all the calculations the following indices of refraction of glass, polystyrene, and water were $n_g = 1.50$, $n_{ps} = 1.59$, and $n_w = 1.33$, respectively. The particle diameter was always 0.489 μm and the laser wavelength in air was 514 nm. Mie calculations agreed with the value of l^* obtained from the simulations ($l^* = 22$ μm).

Figure 5 shows nine different simulation perpendicular displacement distributions $2\pi\rho Q(\rho)$ each for a different window thickness and each plotted against perpendicular displacement length ρ. The peak indicated in this $2\pi\rho Q(\rho)$ distribution will cause a slope discontinuity, or kink to appear in the CB cone. Say this perpendicular displacement length peak occurs at a distance Δ; then the cone-building integral [Eq. (2.2)] $\int 2\pi\rho Q(\rho) J_0(q_\perp \rho) d\rho$ will make a strong negative contribution when $J_0(q_\perp \Delta)$ goes to its most negative value, which occurs when $q_\perp \Delta = 2\pi\theta_{\text{kink}}\Delta/\lambda = 3.83$. It is in this way that the kink angle θ_{kink} can be predicted. Very little light is reflected back into the sample until the critical angle for total internal reflection is reached. Therefore this peak in $Q(\rho)$ induced by the window should occur at $\Delta \approx 2D\tan(\theta_{\text{crit}})$ with D the glass window thickness. The arrows in Fig. 5 indicate this prediction.

Figure 6 includes experimental and simulated cones from identical colloidal samples each with a different thickness of glass at its boundary. Figure 6(a) is the experimental result. In all of Fig. 6 the open circles are a prediction from our scattering simulation (Fig. 5's peak) of the location of a cone slope discontinuity due to a reflection-induced peak in the path length distribution $Q(\rho)$. Figure 6(b) is our simulation's cones which

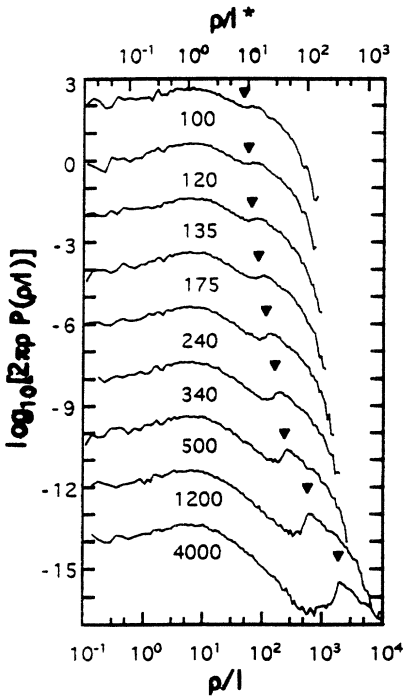

FIG. 5. Plot of the logarithm of the simulation's annular probability for a multiple scattering path to have a given perpendicular displacement (projected length between the first and last scatterer perpendicular to the inbound laser beam). The mean free path l of a photon in the polystyrene medium consisting of 10% volume fraction 0.489 μm diam spheres is found from the Mie theory to be 3.9 μm, while the transport mean free path l^* is 22 μm. Note the two peaks in the distributions. The first occurs at $\rho \approx l^*$ as predicted by the diffusion approximation. The second is due to the reinjection of photons trying to leave the sample at angles greater than the critical angle. Very little light is reflected back into the sample until the critical angle for total internal reflection is reached. Therefore this second peak in $Q(\rho)$ induced by the window should occur approximately at the arrow's location $\Delta \approx 2D\tan(\theta_{\text{crit}})$ with D the glass window thickness. The numbers adjacent to each curve are glass thicknesses in micrometers.

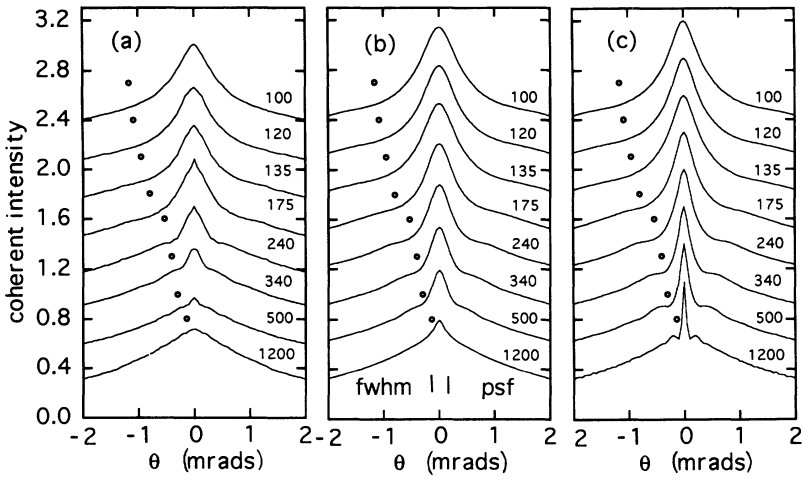

FIG. 6. Coherent intensity vs scattering angle for (a) experimentally observed, circularly averaged backscattering cones for eight different windows whose thicknesses are indicated next to each curve in micrometers. (b) Simulation-derived cones obtained by Fourier transforming the computer simulation's perpendicular displacement distribution function $Q(\rho)$ shown in Fig. 5. The cones in (a) and (b) have been convolved with the experimental point spread function, whose FWHM is equal to 0.25 mrad. (c) Unconvolved simulation cones for which the coherent intensities all reach a normalized value of 1. In each case the open circles correspond to our computer backscattering simulation's prediction of the location of a cone slope discontinuity due to a peak in the simulation's perpendicular displacement distribution $Q(\rho)$.

have been convolved with our experimental 0.25 mrad full width at half max (FWHM) point spread function (PSF). Figure 6(c) is the unconvolved simulation result, shown to demonstrate the effect of the point spread function. Note that there are no free parameters in the simulation. Thicker window glass causes longer single reflection photon transport, which in turn results in longer perpendicular displacements for the reflection-sourced cone part. This cone part is then confined to a smaller and smaller angular width, which the PSF then more severely attenuates. At 100 μm glass thickness the PSF effect causes a loss of only 7.5% of cone height, while for 1200 μm glass the height attenuation approaches 40%. Figure 7 plots CB cone height versus sample window thickness demonstrating that when a significant amount of perpendicular transport of the reflected light occurs the cone height will be greatly diminished.

In the experiment, we used an optical quality BK1 glass window 4 mm thick and a 12 mm sample aperture. Point spread functions were taken with and without the 4 mm thick BK1 glass and no degradation of the PSF was observed. This was not always the case for lower quality glasses such as cover glasses and microscope slides. Figure 8 demonstrates how a quartz cuvette sample cell will also diminish the height of the experimental cone. This cuvette cell, similar to one used in other studies [18], has a window thickness of 1.2 mm and was illuminated with a beam of 8 mm diameter. The cone from such a sample will resemble the lowermost cone of Fig. 6(c), where the sharply peaked portion is due to the light reflected from the air-glass interface. As explained in the preceding paragraph the PSF will then severely attenuate this central section of the cone. The result is cone m, which has a coherent height of only 0.6. In contrast, cone l is obtained with the same sample, but here contained by an apertured, optical quality 4 mm thick window, said aperture prevented the reflected light from returning to the sample. The result was a cone with a coherent height of 0.8. When m was stretched, cones l and m were found to be almost identically shaped, except for the small angle central region. This is because the high angle portion of the cone comes from light that directly left the sample without being reflected. The very sharp, low angle portion of the cone arises from reflected light and would severely distort the cone as shown in Fig. 6. However, this sharp portion of the cone is eliminated by the instrumental point spread function.

Cone n is a V-H cone using the optical quality BK1

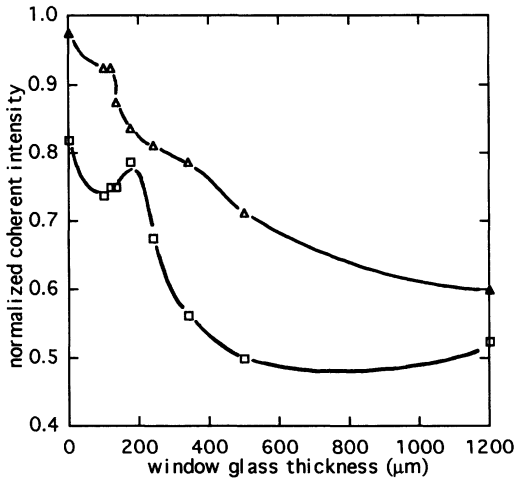

FIG. 7. The normalized coherent intensity of the coherent backscattering cone as a function of window thickness. The triangles depict our simulation cones' heights which are attenuated by convolvement with our experimental 0.25 mrad PSF. The squares indicate the respective cone heights for our experimental cones. The two curves are guides for the eye.

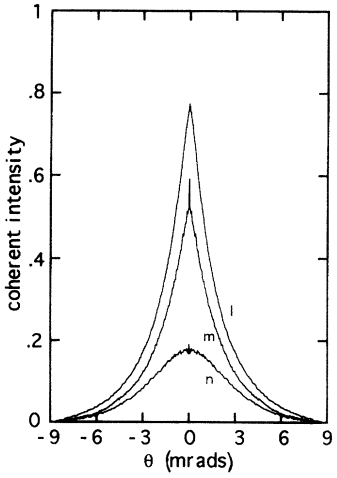

FIG. 8. Cone l is our experimental circularly averaged result for which the reflected light is blocked from returning to the sample (same cone as Fig. 3) achieved by aperturing the colloid-glass boundary of optical quality 4 mm thick glass to 10.5 mm. Cone m results from the same sample contained in a quartz cuvette with a window thickness of 1.2 mm. Note the large degradation in cone height. Cone n is a V-H cone using the same sample and cell as cone l.

glass window. It is shown for completeness and has a coherent height of only 0.2 .

C. Experiment versus simulation versus theory

Figure 9(a) compares simulation and experiment. Cone s is a simulation which ignores reflection from the interface and cone e is our experimentally measured, circularly averaged cone, which best mimics the no reflection condition. Experimentally, the no reflection condition is obtained by aperturing the sample at the colloid-glass interface, thus ensuring that a photon being totally internally reflected from the air-glass interface will be prevented from reentering the sample [8]. We note a remarkable agreement between the simulation and experiment. To compare with the scalar theory the height of the experimental cone had to be stretched from 0.8 to 1 because experimental Mie sphere cones simply do not reach a coherent height of 1.0 [3,4,16,17]. This particular one parameter fit is common practice [4,16,18] and results from the assumption that an extra background signal is responsible for the coherent portion of the CB cone to be less than one. Backgrounds with only our optical quality BK1 glass window present (diffuse scattering sample absent) were indistinguishable from the room's dark level. The implication is that a significant extra background (of order 10%) is present coincident with the presence of the sample in the laser beam. den Outer *et al.* [11] employing the van Albada difference cone technique makes a very strong case that the sample interface is responsible for an extra background of this order of size. Their technique was to take a thin sample of small albedo (several l^* thick) and to subtract its backscattering from that of a thicker sample of the same material which thus had a larger albedo. The resulting "difference" cone representing only the high order scattering paths, having just removed the shorter ones residing at the interface, reached a coherent height of 1.

Figure 9(b) compares three theoretical cone predictions ignoring reflection to our simulation's result [and because of Fig. 9(a)'s agreement, also to experiment]. It is seen that Akkermans, Wolf, and Maynard's [12] "best" theory

$$\alpha(\theta)_{\text{best}} = 3/(8\pi)(1+2z_0/l^* + (1+q_\perp l^*)^{-2} \times\{1+[1-\exp(-2q_\perp z_0)]/(q_\perp l^*)\}) , \quad (3)$$

$$\alpha(\theta)_{\text{approx}} = 3(l^*+z_0)/(2\pi l^*) \times(1+\{1-\exp[q_\perp 2(l^*+z_0)]\}/ \times[q_\perp 2(l^*+z_0)]) , \quad (4)$$

with $q_\perp l^* \approx 2\pi\theta l^*/\lambda$ ($l^* = 22$ μm, $\lambda = 0.514$ μm), plotted as cone b, gives a good zero parameter fit to cone s, our simulation result, and a good one parameter fit (cone height) to our experimental cone e. Akkermans, Wolf, and Maynard's "approximate" theory, cone a, assumes equal depths of the first and last scatterers and fails to fit our experiment's cone wings well, while the

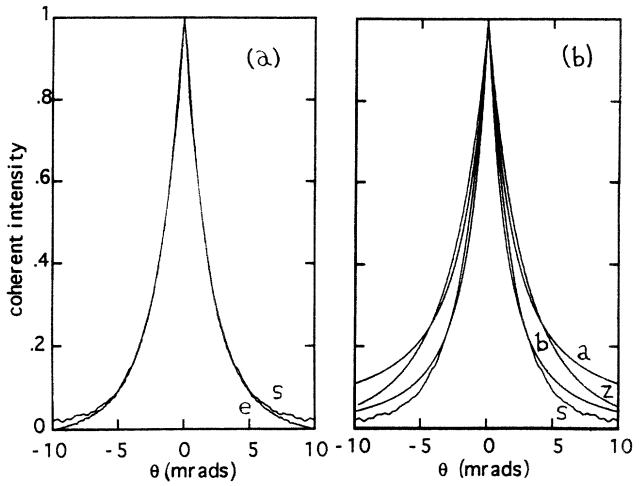

FIG. 9. A comparison of coherent backscattering cones, all of which ignore interface reflection and have an $l^* = 22$ μ. (a) Cone s is our simulation result. Cone e is the circularly averaged experimental cone of Figs. 3 and 8 stretched from 0.8 to 1 in height and having set its background at 10 mrad to zero coherent intensity. The sample was apertured in order to prevent interface reflection as described in the text. (b) Cone a is Akkermans, Wolf, and Maynard's [12] approximate theory's prediction (equal depth of the first and last scatterers at one l^* into the medium). Cone b is their best theory (here first and last scatterer's depths are exponentially damped). Cone z is the Zhu-Pine-Weitz [7] approximate theory's prediction. Cone s is our simulation result. $l^* = 22$ μ corresponds to a 10% volume fraction colloidal suspension of 0.489 μm diam polystyrene spheres having an index of refraction of 1.59, suspended in water, and illuminated with a 514 nm green laser line.

"best" theory accounts for an exponential distribution of depths for the entering and exiting photons. Akkermans, Wolf, and Maynard's theory employs the Milne equation [4,23] with a trapping, or mirror plane, located at $z_0 = 0.71l^*$ (here = 15.6 μm) outside the medium. Interestingly, this choice of z_0 in the Akkermans, Wolf, and Maynard's best theory gives a good zero parameter fit to our simulation and one parameter fit (stretching the coherent cone height to from 0.82 to 1) to our experiments. However, our simulation matches the wings of the experimental cone a bit better then the diffusion approximation, perhaps because the simulation handles the boundary conditions more precisely.

D. Reflection versus no reflection

Figure 10 shows simulated distribution functions for the perpendicular displacement between entering and exiting photons $2\pi\rho Q(\rho)$ plotted versus perpendicular displacement ρ (in units of both l and l^*). For these simulations the samples were "windowless" (zero interfacial thickness) and were composed of 10% volume fraction polystyrene in water. The dotted curve ignores interface reflection, while the solid curve includes interface reflectivity. The average reflectivity, calculated from the simulation by integrating over all scattering angles, was 41%. The same result is obtained theoretically by assuming a Lambertian distribution of scattered light and summing the angle-dependent reflectivity over all angles.

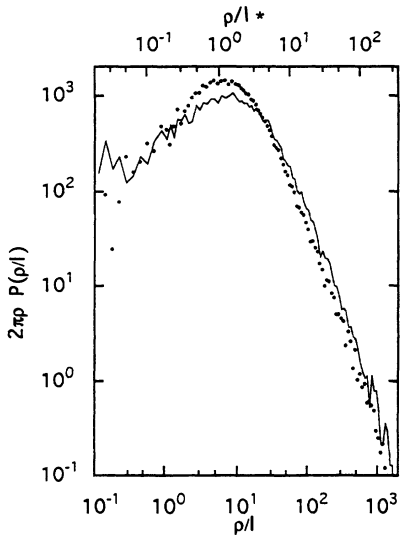

FIG. 10. Two simulation perpendicular displacement probability distribution functions $[2\pi\rho Q(\rho)]$ in a log-log plot as a function of the number of mean free paths (l) and transport mean free paths (l^*). The dotted curve ignores interface reflection, while it is included for the solid curve. In each case the samples are windowless and are composed of polystyrene spheres in water at 10% volume fraction. The peak in the distribution ignoring reflectivity occurs at $\rho \approx l^*$ and the distribution has slope -2 for $\rho \gg l^*$ as predicted by the diffusion approximation [12].

This plot also indicates that the probability of having paths forming closed loops or $\rho \ll l^*$ is small because the ρ distribution falls off as ρ^{-1} below $\rho = l^*$. This simulation result implies that angle-independent scattering from closed loops is improbable for scalar Mie scatterers.

In Fig. 11 are plotted total path length distribution functions. Note that the total path length distribution for the case ignoring reflectivity has a slope of -1.5 as expected from the diffusion approximation [12]. Including reflectivity displaces perpendicular displacement probability outwards from the central peak.

It is interesting to observe that the medium's boundary itself (not the window) could be responsible for an additional cone height loss. In our Fig. 10 we showed a peak in the perpendicular displacement (ρ) distribution at $l^* \approx 20\mu$ and a falloff going like ρ^{-2}, both consistent with the diffusion approximation. Also in our Fig. 6 we showed how the mechanism of perpendicular photon transport at the interface would cause cone height loss. A 100 μm thick window would cause $\sim$ 40% of the photons to be perpendicularly transported approximately 200 μm $\approx 10l^*$, netting a 7.5% cone height loss when convolved with the experimental resolution function. Note that our experimental point spread function would be responsible for a height loss of only order 2.5% were the interface completely transmitting and the perpendicular displacement distribution undistorted.

Our sample is a 10% volume fraction charged, polystyrene (PS) colloid, with the PS itself repelling from the like-charged glass window. A photon exiting this colloid "sees" not just water→glass then glass→ air interfaces, but first sees a graded colloid→water interface, a gradation in the index of refraction from high to low (GRIN effect) during which the number of PS scatterers

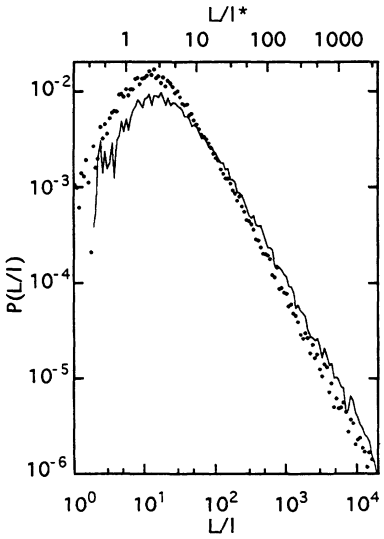

FIG. 11. Log-log plot of total path length distribution functions $Q(L)$ from the same simulations as Fig. 10 ignoring interface reflection (dotted line) and from a simulation including reflection (solid line). The no reflection curve has a slope of -1.5 for $L \gg l^*$ as predicted by the diffusion approximation [12].

drops towards zero and internal reflection is encouraged. The distance over which the density of the colloid varies from the glass surface to the bulk is likely to be several microns at most (5–10 particle diameters) for the suspensions used in our study. It is not clear how much perpendicular transport of light would occur in such a thin layer or how the structure of the layer would effect this transport. Further theoretical work is needed to evaluate this proposed mechanism for loss of cone height.

Another interesting boundary effect occurring in the simulation became apparent when measuring the simulation's interface reflectivity by counting the numbers of photons reflecting 0,1,2,... times. Here 41% of the photons reflected at least once; however, a single reflection was found to increase the likelihood of subsequent reflections (all higher order reflection probabilities were $\approx$ 50%). A photon reflecting once at the critical angle reenters the medium at approximately a 40° angle to the interface. Because these are Mie spheres they scatter essentially forward into a small cone (< 60° apex angle). Here because the photon's scattering cones are "angularly close" to the surface the photons are more likely to rescatter off of it. Compare this against the initial photon entering at a 90° angle to the interface being "angularly far" from the surface and thus having a lower reflection probability. This effect is an interaction occurring on a distance scale $l < l^*$ between an angle-dependent Mie sphere scattering and an angle-dependent Fresnel interface reflectivity.

Figure 12 shows the cones constructed from the perpendicular displacement distributions. The reflection simulation cone (41% average angle-dependent Fresnel reflectivity) has a full width half maximum 68% of the simulation cone ignoring reflection. Lagendijk *et al.* [6] predict that the FWHM should shrink to ~76% of the no-reflection FWHM for a 41% interface reflectivity (their $z_0 = 0.71l^*$). Freund and Berkovits's theory [8] predicts the FWHM shrinking to ~ 64% of the no-reflection FWHM for the same situation.

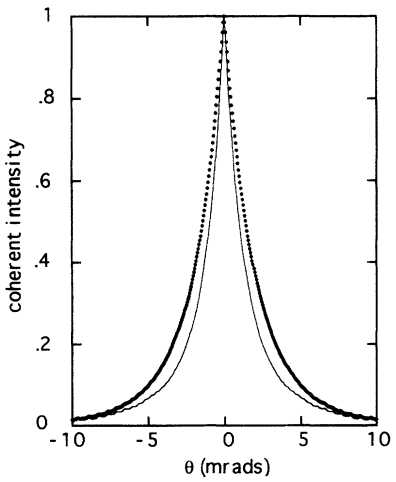

FIG. 12. The simulation coherent backscattering cones corresponding to the perpendicular displacement distribution function of Fig. 10. Again the dashed curve corresponds to ignoring reflection and the solid curve to a 41% average interface reflectivity. Lagendijk *et al.* [6] predict a 41% reflection cone to have 76% the FWHM of the cone without interface reflectivity, while Freund and Berkovits [8,24] predict 64%, and our simulation of an angle-dependent interface reflectivity returns a 68% result.

Figure 13 is a comparison of Lagendijk, Vreeker, and DeVries's [6] graph of the cone FWHM versus internal reflectivity R (here $z_0 = 0.71l^*$, called the Milne result, corresponding to $R = 0$) together with Freund and Berkovits's [8,24] cone FWHM versus reflectivity R, and 16 data points of the FWHM vs R from our computer simulation. It is important to observe that z_0 should increase as R is increased [24]. Also it appears that Freund and Berkovits's theory [their Eq. (3), our [8]] captures the essential physics of shrinking cone width with increasing R. Here we reproduce the main part of their Eq. (3):

$$\gamma(R) = (1 - R)\gamma_0/(1 - R\gamma_0) \ , \tag{5}$$

where γ_0 is the CB shape function in the absence of reflection, and $\gamma(R)$ is the corrected-for-reflection CB shape function. One should note that Lagendijk, Vreeker, and DeVries's [6] and Freund and Berkovits's [8,24] reflectivity's R are not angle dependent, while our reflectivity R is an angular average of the Fresnel reflectivity for a Lambertian scatterer for which the scattered intensity varies as $\cos\theta$ ($R \approx 2\int_{\theta=\theta_{\rm crit}}^{\theta=\pi/2} \cos\theta \sin\theta \, d\theta$). Our simulation's curve exhibited a descending staircase structure, which was a reproducible feature and not a consequence of statistical fluctuations.

E. Sample aperture versus cone height

Allowing nonilluminated regions of the sample to return scattered flux to the detector will cause the cone height to diminish. This occurs because these regions fail

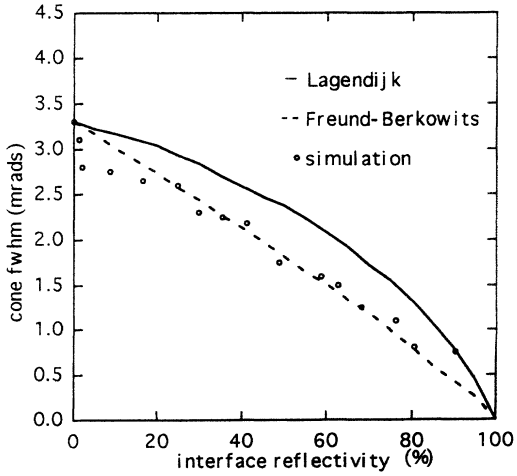

FIG. 13. Comparing Lagendijk, Vreeker, and DeVries's [6] functional form of cone width (FWHM) versus internal reflectivity R ($z_0 = 0.71l^*$), with Freund and Berkowits's theory's [8,24] FWHM vs R, and our 16 simulation cones' FWHM vs R.

to provide time-reversed partners. This effect is similar to illuminating the random medium with a small diameter laser beam [25]. Figure 14 is an experimental series of cones where the beam size is fixed and the sample aperture is varied. In each case an 8 mm diam laser beam struck the colloid through a 4 mm thick BK1 glass window. The sample was apertured at the colloid-glass interface using black absorbing tape. Improvement in cone height was subtle as aperture was decreased and effectively ceased as sample aperture was reduced through 10.5 mm. This 10.5 mm aperture removed the large population of long perpendicular displacement, interface-reflected photons, significantly improving the CB cone. Figure 14 demonstrates that the larger apertures such as 16 and 20 mm allowed long perpendicular displacement light loops to miss their time-reversed partners. The cone then suffered losses inside an angular width of 2 mrad.

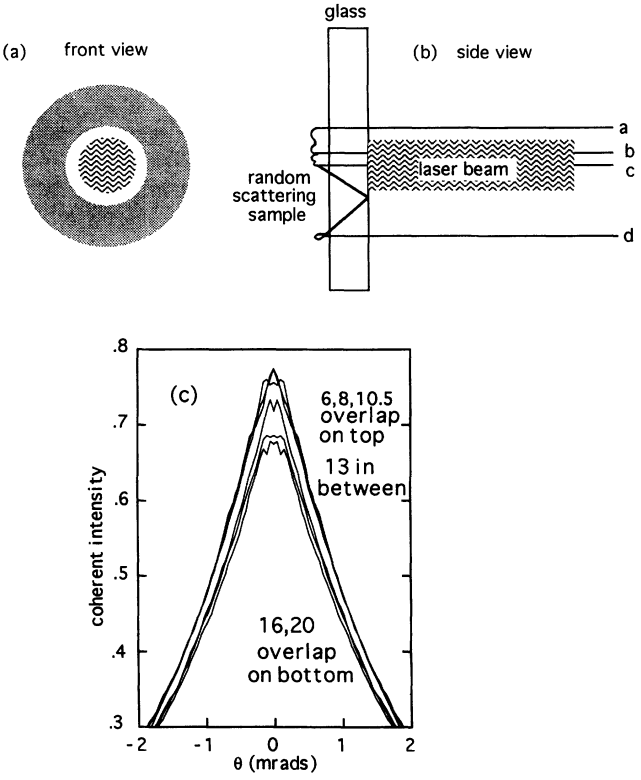

FIG. 14. (a) A laser beam's eye view of the air-glass interface. The central wavy circle represents our 8 mm diam laser beam. The outer, shaded annulus corresponds to totally internally reflected light, which has no time reversed partners. The average radius $(R_{outer}+R_{inner})/2$ of the shaded annulus is $2D\tan(\theta_c)$, with D the glass thickness and θ_c the glass-air critical angle [29]. (b) A side view of the laser beam impinging upon the same air-glass random sample interface. Backscattering loop *bc* would contribute both a partner and time-reversed partner amplitude to a detector hit, while loop *ba* would be lacking a time reversed partner amplitude. A loop *bd* backscattering photon would experience the large perpendicular transport incurred by a glass-air internal reflection and would also lack a time-reversed partner amplitude. (c) Plotted are the coherent portion of six cones, each using an 8 mm laser beam illuminating a 4 mm thick optical quality BK1 glass sample cell. The colloidal medium-glass interface is then apertured so that nonilluminated sample regions having no time-reversed partners could return flux to the detector. Cones improved in a subtle way as aperture size was decreased. Cone improvement ceased at a 10.5 mm aperture because this width prevented the large population of internally reflected photons from scoring detector hits. Aperturing away the smaller population of photons corresponding to loops such as *ba* had little benefit in improving the cone (the numbers refer to sample aperture diameter in millimeters).

F. Diffusing-wave spectroscopy experiment

A diffusing-wave spectroscopy experiment was carried out on our 10% volume fraction, 0.489 μm sphere-diameter colloidal sample, said sample apertured to 12 mm. The field autocorrelation function $g_1(t)$ [7,26] was measured for three different window thicknesses of the sample. The measurement was taken in a backscattering geometry at 170° with respect to the illuminating laser beam. For backscattering $g_1(t) \approx \exp(-\gamma\sqrt{6t/\tau})$, where γ is a function of polarization, interface reflectivity, and the ratio l^*/l [7]. $\tau = 1/Dk^2$ is a time constant associated with diffusing Brownian particles, where D is the particle diffusion coefficient and k is the magnitude of the light's wave vector in the sample [7].

Figure 15 shows the decay of this field autocorrelation function $g_1(t)$ in a log-lin plot versus the normalized square root of time for three different window glass thicknesses. The decay rate of $g_1(t)$ is governed by the cumulative motion of each of the scatterers in a given path. Thus long paths decay faster than short ones. With thin windows, most of the reflected light returns to the sample, which increases the average path length. In contrast, light reflected from thick windows lands outside the sam-

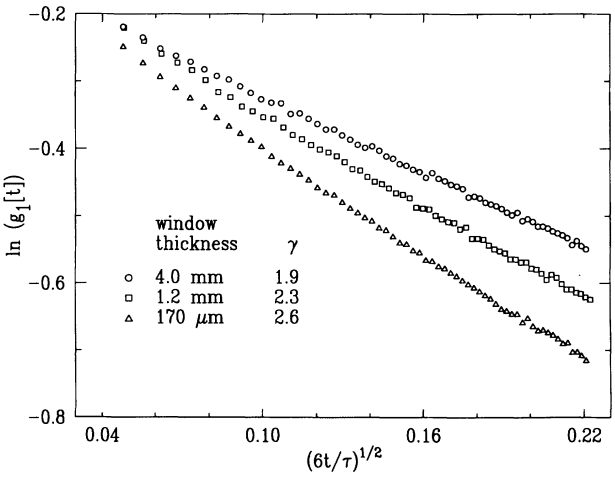

FIG. 15. A log-lin plot of the field autocorrelation function $g_1(t) \approx \exp(-\gamma\sqrt{6t/\tau})$ versus the normalized square root of time. More reflected light is returned to the sample for the thin windows than for the thick ones. This lengthens the total path length of the light in the sample and leads to an increase in the decay rate for thin windows, compared to thick.

ple and is absorbed. This guarantees that the backscattered light escaping the cell has only been in the sample once and therefore that the decay of $g_1(t)$ will be less for thick windows than for the case of thin windows. Experimentally, we observed that γ varied from 2.6 for a thin window to 1.9 for a thick window. The integral equation formalism of MacKintosh and John [27,28] makes a theoretical prediction $\gamma_{\|} \approx 2$ for Mie spheres, close to the observed value for the thick window.

III. CONCLUSIONS

A significant coherent backscattering cone anisotropy holds for the Mie sphere as well as for the Rayleigh sphere case for the low orders of V-V geometry multiple backscattering.

It is seen that one can create a peak in the path length distribution of the multiple scattering whose position is determined by the window thickness of the sample cell. A CB cone slope discontinuity results whose angular position is well predicted by the location of this peak in our computer backscattering simulation, demonstrating the importance of including reflectivity from interfaces in treatments of the CB cone.

The presence of this slope discontinuity in the CB cone is associated with a new mechanism of reducing cone height: perpendicular photon transport at the exit interface will distort the distribution of perpendicular displacements, causing a disproportionate number of photons to have large displacements. This group of photon's contribution to the CB cone will then be attenuated by the point spread function.

Monte Carlo simulations of ballistic photon transport, which go beyond the diffusion approximation by using accurate boundary conditions, show an excellent one parameter fit to our experimental cone measurement for which the reflected light was eliminated. The cone height fitting parameter is necessary because of the experimental Mie sphere cone's failure to reach a coherent height of 1.0. Likewise our simulated cone, ignoring reflection, makes a good zero parameter fit to the Akkermans, Wolf, and Maynard's [12] "best" theory, if one uses the Milne equation's result for mirror plane location ($z_0 = 0.71l^*$).

Our simulation of CB cones from a medium interfaced with an angle-dependent reflectivity shows a smaller cone width for a given reflectivity than does the theory of Lagendijk *et al.* [6], which describes the shrinking of cone angular width with increasing angle-independent interface reflectivity (a somewhat unfair comparison because we are supplied only with a curve having $z_0 = 0.71l^*$, while z_0 is known to increase with increasing reflectivity). Our simulation appears to fit better to Freund and Berkovits's theory [8]. This is in contrast to the experiments of Saulnier and Watson [10], who find a better agreement for the theory of Lagendijk *et al.* [6]. The simulation's cone width versus interface reflectivity curve also has an interesting stair step structure.

Two sources of experimental cone height loss are accounted for. Whenever the cone's apex angle is very sharp (such as caused by a thick glass window boundary condition) the point spread function will severely attenuate cone height and a large loss of height will result. A second loss of cone height occurs whenever nonilluminated sample regions are permitted to return backscattered flux to the detector. By properly aperturing the sample, both loss mechanisms can be minimized, and a 0.82 coherent cone height was obtained using Mie scatterers. Implied is that there still remains a significant extra background of order 10% present coincidentally with the presence of the sample in the laser beam. This extra background could be due to the action of unaccounted for angle-independent scattering loops, to a cooperative scattering between terms residing along the interface referred to as a diffuse-specular by den Outer *et al.* [11], to significant perpendicular photon transport at the exit interface, or could have an experimental origin such as scatter from optical components. However, our simulation indicates that it is improbable for photons to exit from the sample with a small displacement from the entering point and hence that angle-independent scattering loops are not likely responsible for the extra background.

The field autocorrelation function $g_1(t) \approx \exp(-\gamma\sqrt{6t/\tau})$ decays slower with thicker glass windowed samples, which have been apertured, than with thin windows. This is because the reflected light from thin windows returns to the sample and lengthens the path length distribution.

ACKNOWLEDGMENT

We thank Brandeis University for financial support of this project.

[1] Y. Kuga and A. Ishimaru, J. Opt. Soc. Am. A **1**, 831 (1984); L. Tsang and A. Ishimaru, *ibid.* **1**, 836 (1984).
[2] M. P. van Albada and A. Lagendijk, Phys. Rev. Lett. **55**, 2692 (1985); P. E. Wolf and G. Maret, *ibid.* **55**, 2696 (1985).
[3] E. Akkermans, P. E. Wolf, R. Maynard, and G. Maret, J. Phys. (Paris) **49**, 77 (1988).
[4] M. P. van Albada, M. B. van der Mark, and A. Lagendijk, *Scattering and Localization of Classical Waves in Random Media*, edited by P. Sheng (World Scientific, Singapore, 1990), p. 97.
[5] M. B. van der Mark, M. P. van Albada, and A. Lagendijk, Phys. Rev. B **37**, 3575 (1988).
[6] A. Lagendijk, R. Vreeker, and P. De Vries, Phys. Lett. A **136**, 81 (1989).
[7] J. X. Zhu, D. J. Pine, and D. A. Weitz, Phys. Rev. A **44**, 3948 (1991).
[8] I. Freund and R. Berkovits, Phys. Rev. B **41**, 496 (1990).
[9] L. Tsang and A. Ishimaru, J. Opt. Soc. Am. A **2**, 2187 (1985).
[10] P. M. Saulnier and G. H. Watson, Opt. Lett. **17**, 946 (1992).

[11] P. N. den Outer, M. P. van Albada, and Ad Lagendijk, in *Photonic Band Gaps and Localization*, Vol. 308 of *NATO Advanced Study Institute, Series B: Physics,* edited by C. M. Soukoulis (Plenum, New York, 1993), p. 75.
[12] E. Akkermans, P. E. Wolf, and R. Maynard, Phys. Rev. Lett. **56**, 1471 (1986).
[13] Cohu 4810 series solid-state CCD camera, Cohu Inc. Electronics Division, 5755 Kearney Villa Road, P.O. Box 85623, San Diego, CA 92186-5623.
[14] Image Grabber digitizer board and software, Neotech Limited, P.O.B. 46, Eastleigh, Hampshire SO5 5UG, UK.
[15] I P Lab image processing software, Signal Analytics Corp., 374 Maple Avenue East, Suite 200, Vienna, VA 22180.
[16] P. E. Wolf, G. Maret, E. Akkermans and R. Maynard, J. Phys. (Paris) **49**, 63 (1988).
[17] M. Kaveh, M. Rosenbluh, I. Edrei, and I. Freund, Phys. Rev. Lett. **57**, 2049 (1986).
[18] S. Fraden and G. Maret, Phys. Rev. Lett. **65**, 512 (1990).
[19] N. W. Ashcroft and J. Lekner, Phys. Rev. **145**, 83 (1966).
[20] M. S. Wertheim, Phys. Rev. Lett. **10**, 321 (1963).
[21] M. P. van Albada, M. B. van der Mark, and A. Lagendijk, J. Phys. D **21**, S28 (1988).
[22] H. C. van de Hulst, *Light Scattering by Small Particles* (Dover, New York, 1957).
[23] B. Davison and J. B. Sykes, *Neutron Transport Theory* (Oxford University Press, New York, 1957); A. Ishimaru, *Wave Propagation and Scattering in Random Media* (Academic, New York, 1978), Vol. 1.
[24] I. Freund (private communication).
[25] P. E. Wolf and G. Maret, in *Scattering in Volumes and Surfaces,* edited by M. Nieto-Vesperinas and J. C. Dainty (North-Holland, Amsterdam, 1989).
[26] G. Maret and P. E. Wolf, Z. Phys. B **65**, 409 (1987).
[27] F. C. MacKintosh and S. John, Phys. Rev. B **40**, 2383 (1989).
[28] D. J. Pine, D. A. Weitz, J. X. Zhu, and E. Herbolzheimer, J. Phys (Paris) **51**, 2101 (1990).
[29] E. Hecht, *Optics* (Addison-Wesley, Reading, MA, 1987), p. 125, Fig. 4.58.

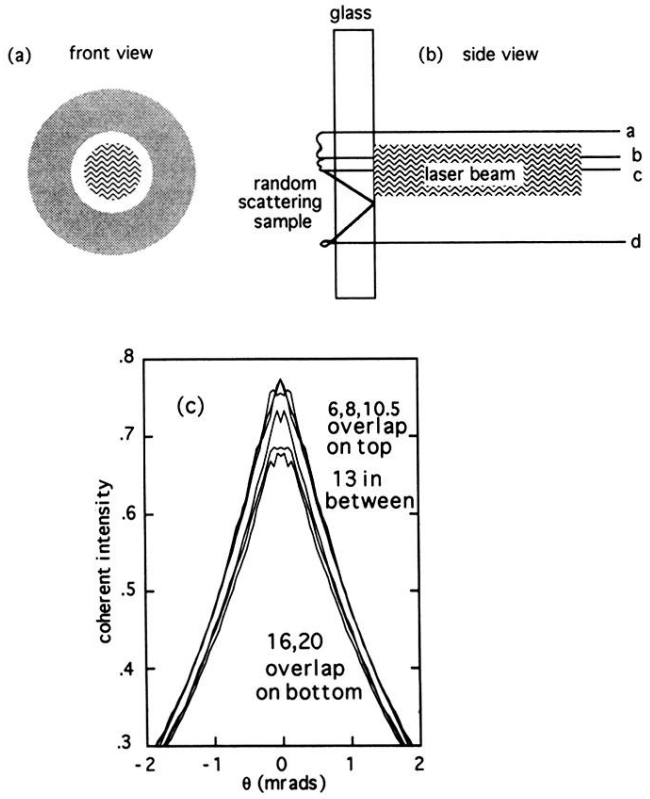

FIG. 14. (a) A laser beam's eye view of the air-glass interface. The central wavy circle represents our 8 mm diam laser beam. The outer, shaded annulus corresponds to totally internally reflected light, which has no time reversed partners. The average radius $(R_{outer}+R_{inner})/2$ of the shaded annulus is $2D\tan(\theta_c)$, with D the glass thickness and θ_c the glass-air critical angle [29]. (b) A side view of the laser beam impinging upon the same air-glass random sample interface. Backscattering loop *bc* would contribute both a partner and time-reversed partner amplitude to a detector hit, while loop *ba* would be lacking a time reversed partner amplitude. A loop *bd* backscattering photon would experience the large perpendicular transport incurred by a glass-air internal reflection and would also lack a time-reversed partner amplitude. (c) Plotted are the coherent portion of six cones, each using an 8 mm laser beam illuminating a 4 mm thick optical quality BK1 glass sample cell. The colloidal medium-glass interface is then apertured so that nonilluminated sample regions having no time-reversed partners could return flux to the detector. Cones improved in a subtle way as aperture size was decreased. Cone improvement ceased at a 10.5 mm aperture because this width prevented the large population of internally reflected photons from scoring detector hits. Aperturing away the smaller population of photons corresponding to loops such as *ba* had little benefit in improving the cone (the numbers refer to sample aperture diameter in millimeters).